JOURNAL CLUB SECOND PART (NUCLEATION & CRYSTAL GROWTH MECHANISMS)

Abel MORENO, Institute of Chemistry, UNAM. MEXICO.

E-mail address: carcamo@unam.mx or abel.moreno@mac.com

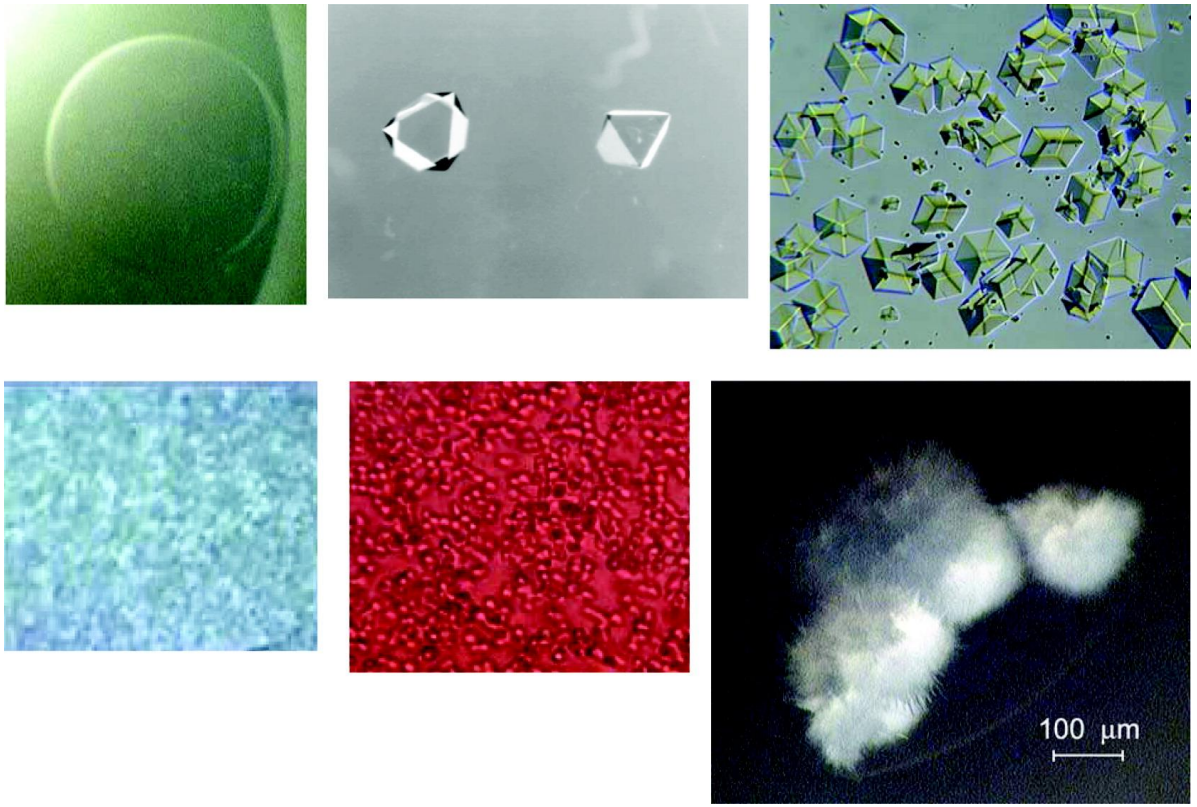

Nucleation largely determines the outcome of crystallization. Examples of protein crystals and other condensed phases illustrate, at top left, the failure of nucleation, where no crystals or other condensed phase is generated in a supersaturated lysozyme solution; and clockwise from there, the nucleation of two crystals of apoferritin, which grow to a relatively large size; the nucleation of numerous crystals of insulin, which have a broad size distribution; needle-like crystals of lysozyme; dense liquid droplets in a solution of hemoglobin A, and, at bottom left, amorphous precipitate in a supersaturated lysozyme solution. Scale bar is shown in bottom right panel.

Published in: Peter G. Vekilov; *Crystal Growth & Design* **2010,** 10, 5007-5019.
DOI: 10.1021/cg1011633

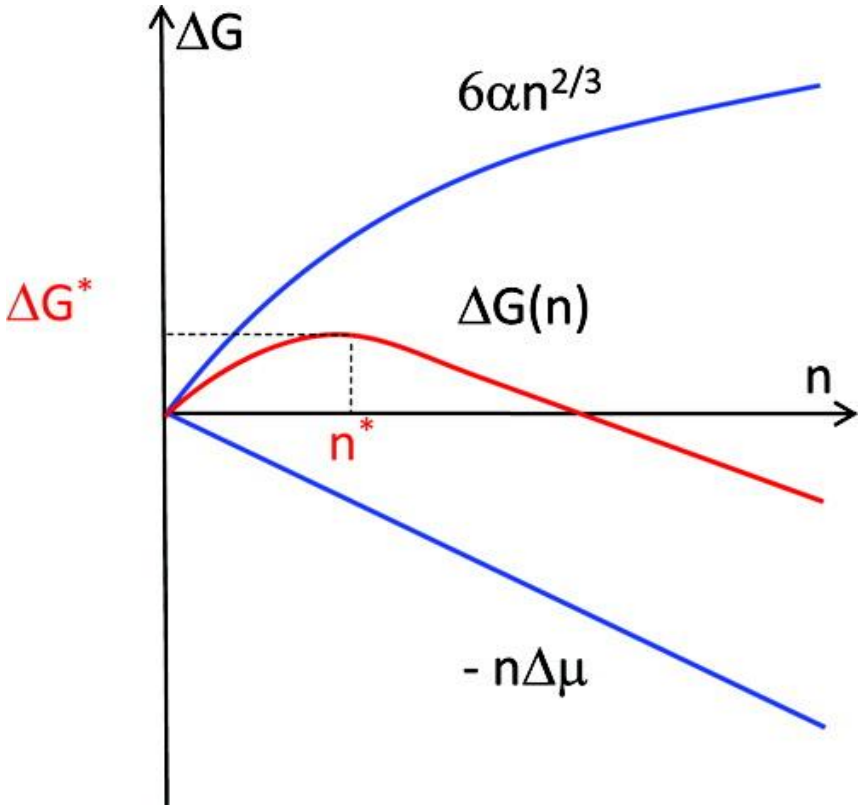

Illustration of the thermodynamic effects of formation of a crystal. n − number of molecules in crystalline embryo; Δμ − solution supersaturation; α − surface free energy; ΔG − free energy; * denotes critical cluster.

Published in: Peter G. Vekilov; *Crystal Growth & Design* **2010,** 10, 5007-5019.
DOI: 10.1021/cg1011633

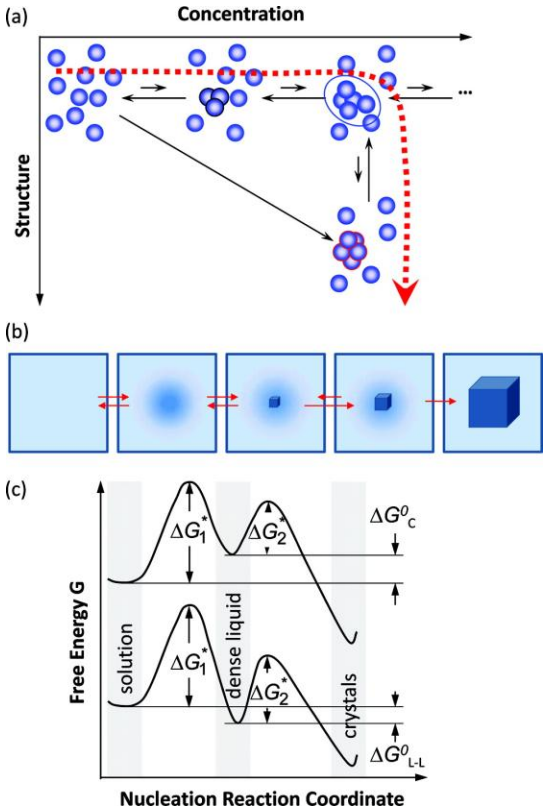

Schematic illustration of the two-step mechanism of nucleation of crystals. A dense liquid cluster forms. A crystal nucleus may form inside the cluster. (a) Microscopic viewpoint in the (Concentration, Structure) plane; (b) macroscopic viewpoint of events along the thick dashed line in (a). (c) The free-energy ΔG along two possible versions of the two-step nucleation mechanism. If dense liquid is unstable and ΔGL−L0 > 0 (ΔGL−L0—standard free energy of formation of dense liquid phase), dense liquid exists as mesoscopic clusters, ΔGL−L0 transforms to ΔGC0, and upper curve applies; if dense liquid is stable, ΔGL−L0 < 0, reflected by lower curve. $\Delta G1^*$ is the barrier for formation of a cluster of dense liquid, $\Delta G2^*$ − for a formation of a crystalline nucleus inside the dense liquid.

Published in: Peter G. Vekilov; *Crystal Growth & Design* **2010,** 10, 5007-5019.
DOI: 10.1021/cg1011633

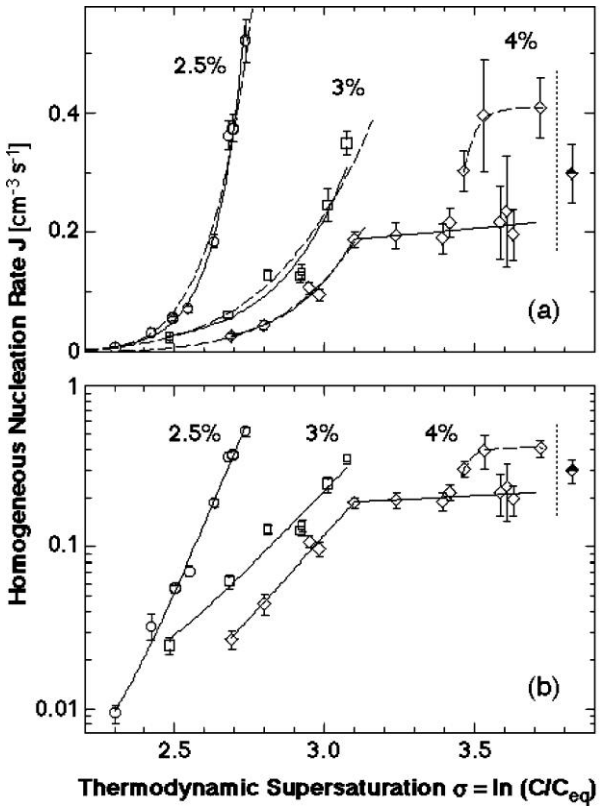

The dependence of the rate of homogeneous nucleation J of lysozyme crystals of supersaturation $\sigma \equiv \Delta\mu/kBT$ at T = 12.6 °C and at the three concentrations of the precipitant NaCl indicated on the plots. Solid lines − fits with exponential functions; dashed lines fits with the classical nucleation theory expression, eq 3. Vertical dotted lines at σ = 3.9 indicate the liquid−liquid coexistence boundary at this T and CNaCl = 4%; this supersaturation corresponds to lysozyme concentration 67 mg mL−1. (a) Linear coordinates; (b) semilogarithmic coordinates. With permission from ref 59. Copyright 2000 American Chemical Society.

Published in: Peter G. Vekilov; *Crystal Growth & Design* **2010,** 10, 5007-5019.
DOI: 10.1021/cg1011633

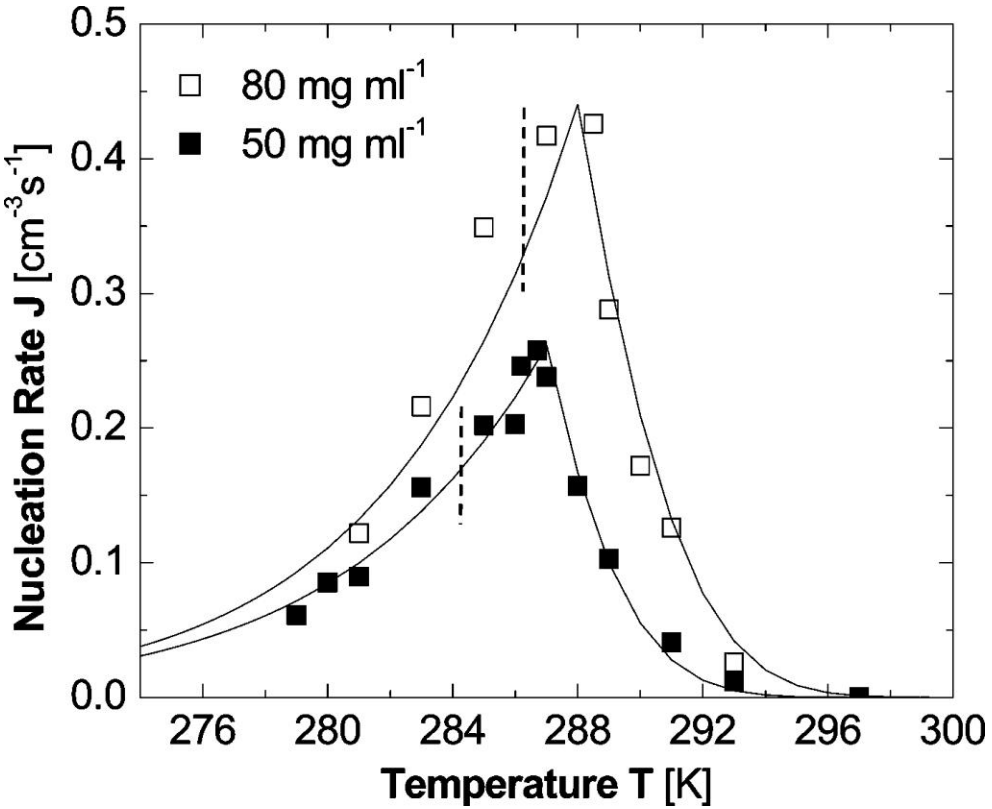

The dependence of the rate of homogeneous nucleation *J* of lysozyme crystals on temperature *T* at two fixed lysozyme concentrations indicated in the plot. The temperatures of equilibrium between crystals and solution are 315 K at *C*lys = 50 mg mL−1 and 319 K at *C*lys = 80 mg mL−1. The temperatures of L−L separation are 285 K at *C*lys = 50 mg mL−1 and 287 K at *C*lys = 80 mg mL−1,(25) and are marked with vertical dashed lines. Symbols represent experimental results from ref 34. Lines are results of two-step model in eqs 5−7. With permission from ref 50. Copyright 2005 American Institute of Physics.

Published in: Peter G. Vekilov; *Crystal Growth & Design* **2010,** 10, 5007-5019.
DOI: 10.1021/cg1011633

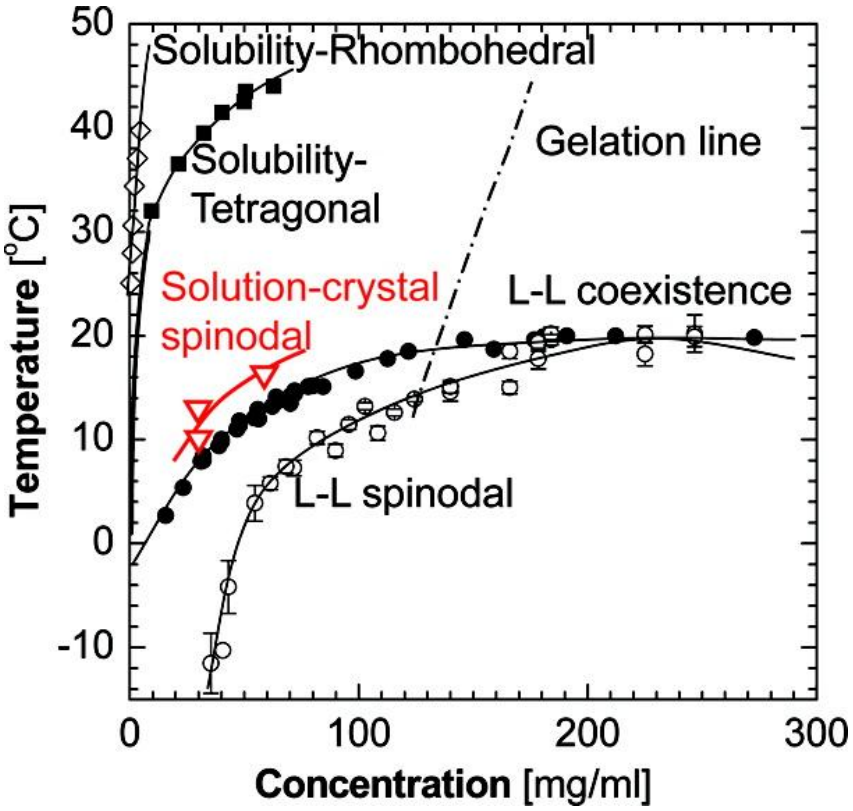

The phase diagram of a lysozyme solution determined experimentally in 0.05 M Na acetate buffer at pH = 4.5 and 4.0% NaCl. Liquidus, or solubility lines—from refs 108 and 109 liquid−liquid (L−L) coexistence and respective spinodal—from ref 25, gelation line—from refs 24 and 25. Solution−crystal spinodal is highlighted in red and is from ref 81.

Published in: Peter G. Vekilov; *Crystal Growth & Design* **2010,** 10, 5007-5019.
DOI: 10.1021/cg1011633

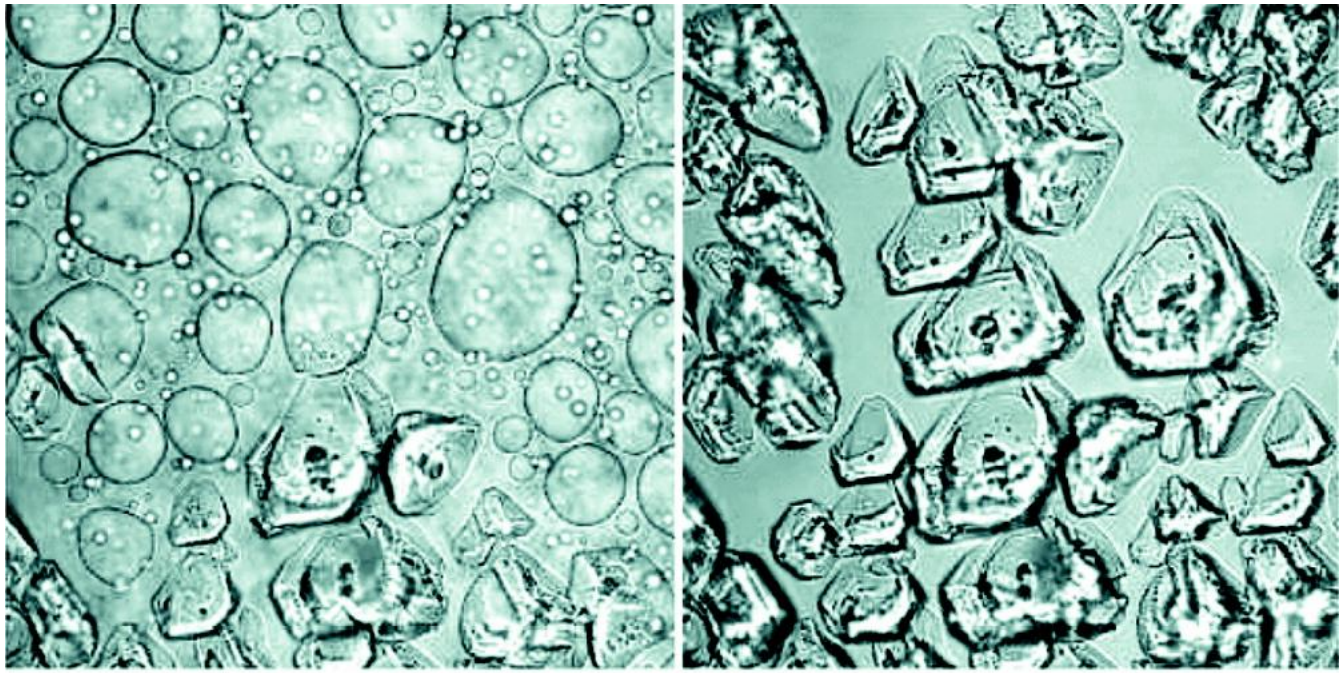

Confocal scanning laser fluorescence microscopy imaging of nucleation of crystals of glucose isomerase within dense liquid droplets. Bright field imaging, polyethylene glycol with molecules mass 10 000 g mol−1 (PEG 10000) used to induce crystallization. The time interval between the left and right images is 380 s. *C*protein = 55 mg mL−1, *C*PEG = 9.5%, 0.5 M NaCl, 10 mM Tris maintaining pH = 7. The width of each image is 326 μm. With permission from ref 64. Copyright 2005 International Union of Crystallography.

Published in: Peter G. Vekilov; *Crystal Growth & Design* **2010,** 10, 5007-5019.
DOI: 10.1021/cg1011633

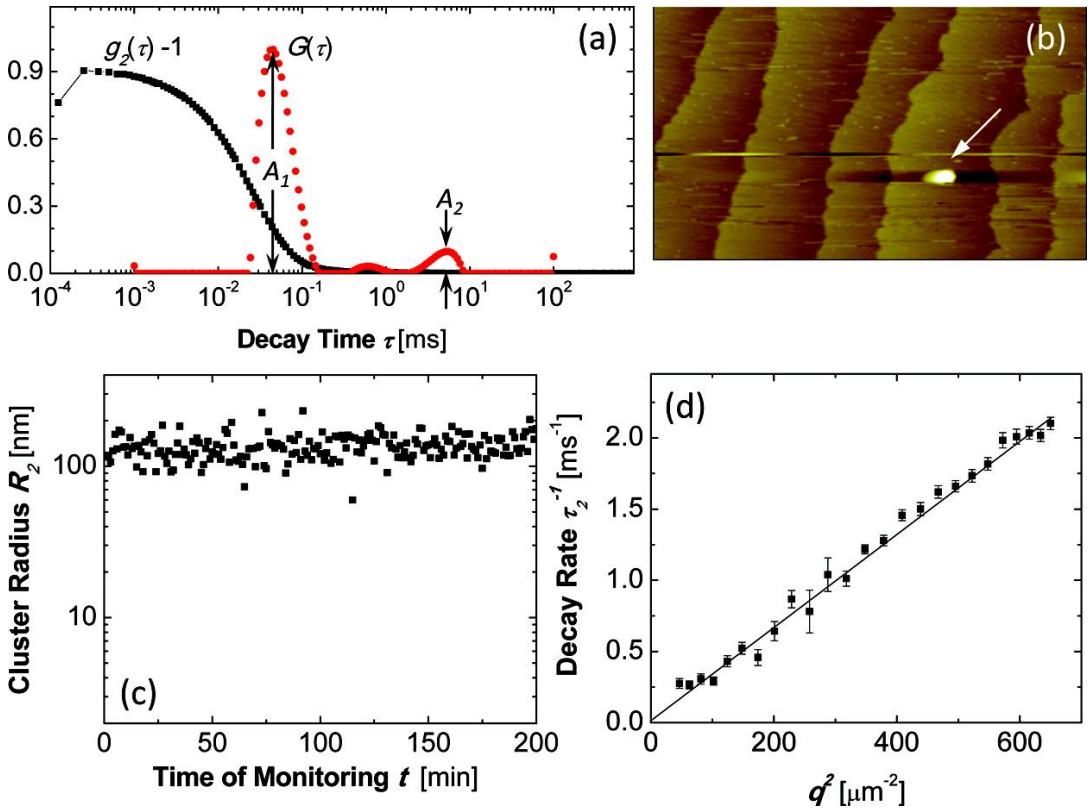

Characterization of dense liquid clusters. (a) Examples of correlation function of the scattered intensity $g2(\tau)$ and the respective intensity distribution function $G(\tau)$ of a lysozyme solution with C = 148 mg mL−1 in 20 mM HEPES buffer; data collected at angle 145°. (b) Atomic force microscopy imaging of liquid cluster landing on the surface of a crystal in a lumazine synthase solution. Tapping mode AFM imaging, scan width 20 μm. Apparent lateral cluster dimensions are misleading; cluster height is 120 nm, with permission from ref 69. Copyright 2005 American Chemical Society. (c) Time dependence of the radius of dense liquid clusters in the same lysozyme solution as in (a). (d) The dependence of the decay rate $\Gamma 2 = \tau 2 - 1$ of the cluster peak in the correlation function on the squared wave vector $q2$ for a lysozyme solution as in (a).

Published in: Peter G. Vekilov; *Crystal Growth & Design* **2010,** 10, 5007-5019.
DOI: 10.1021/cg1011633

Practical Physics Behind Growing Crystals of Biological Macromolecules

(Candoni et al. Proteins and Peptide Letters 2012)

PROTEIN SOLUBILITY: THE FIRST STEP

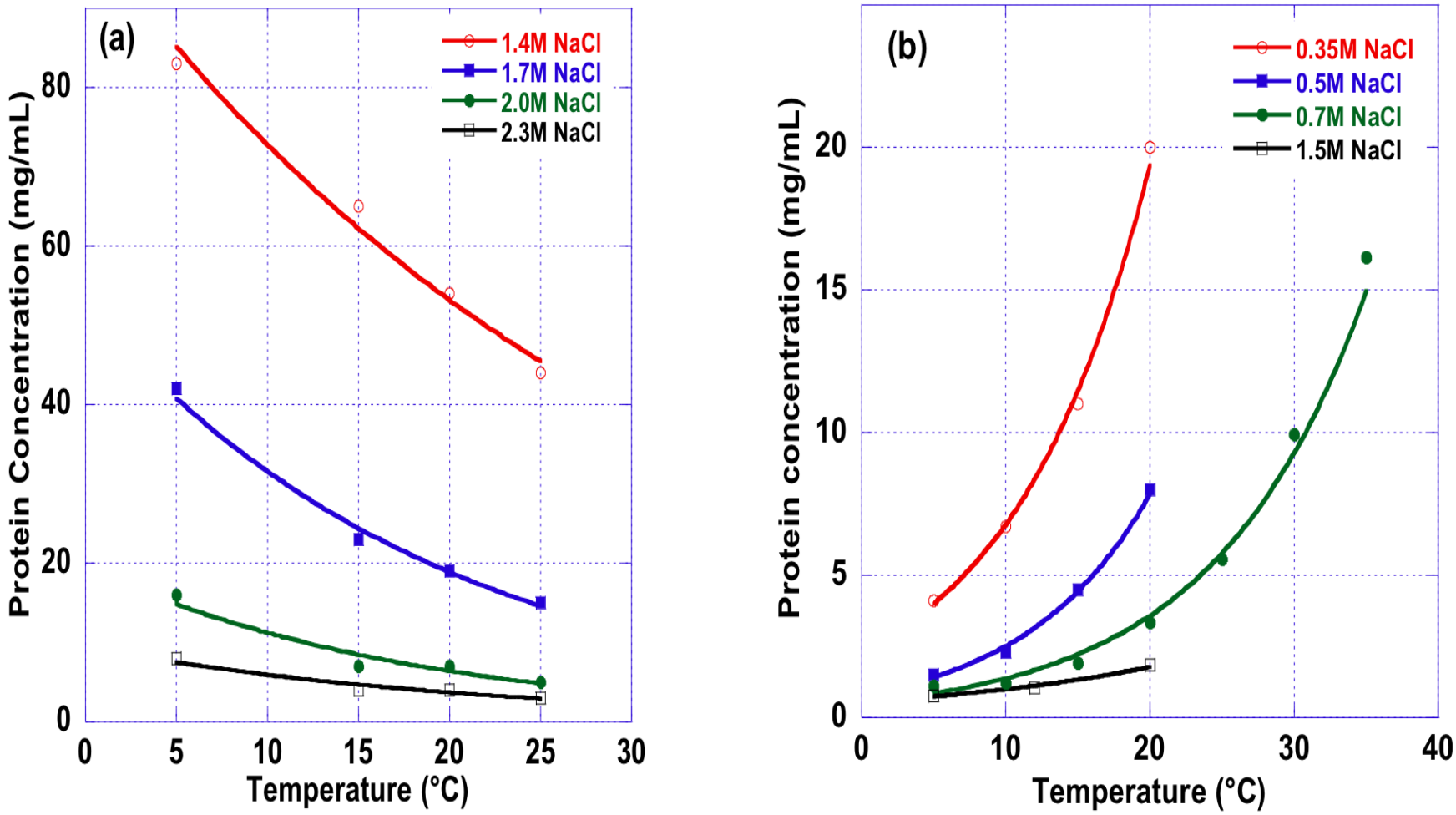

Figure 1: Solubility of (a) BPTI[8] and (b) Lysozyme as a function of NaCl[13] concentrations for different temperatures at pH=4.5. Note the reverse solubility with temperature for BPTI and the direct solubility for Lysozyme.

NUCLEATION: THE BIRTH OF CRYSTALS

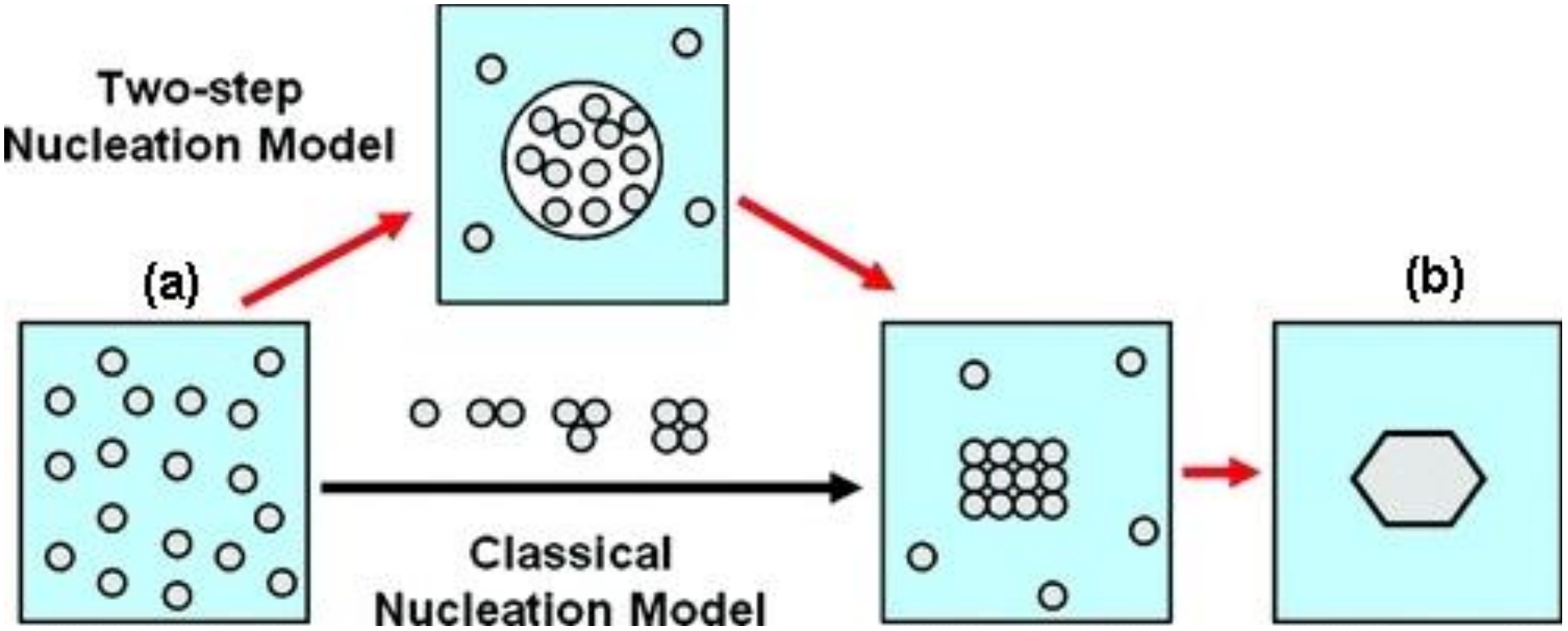

Figure 2: Schematic representation of the different nucleation mechanisms, starting from (a) a supersaturated solution to (b) a crystal. Reprinted with permission from Erdemir et al.[21]. Copyright 2009 American Chemical Society.

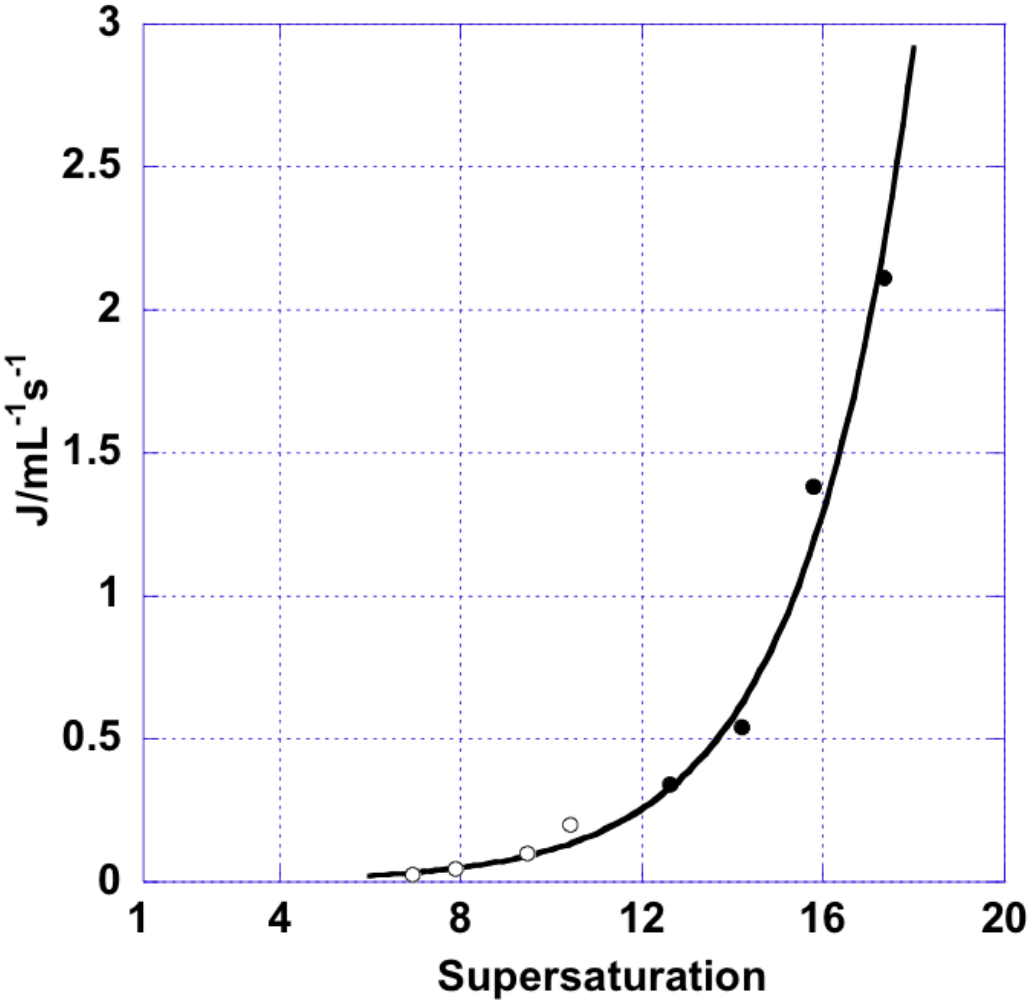

Figure 3: Lysozyme primary nucleation rate vs supersaturation, at 20°C, NaCl=0.7M and pH=4.5 after Ildefonso et al.[27]

GROWTH FORM, GROWTH MEDIUM AND KINETICS

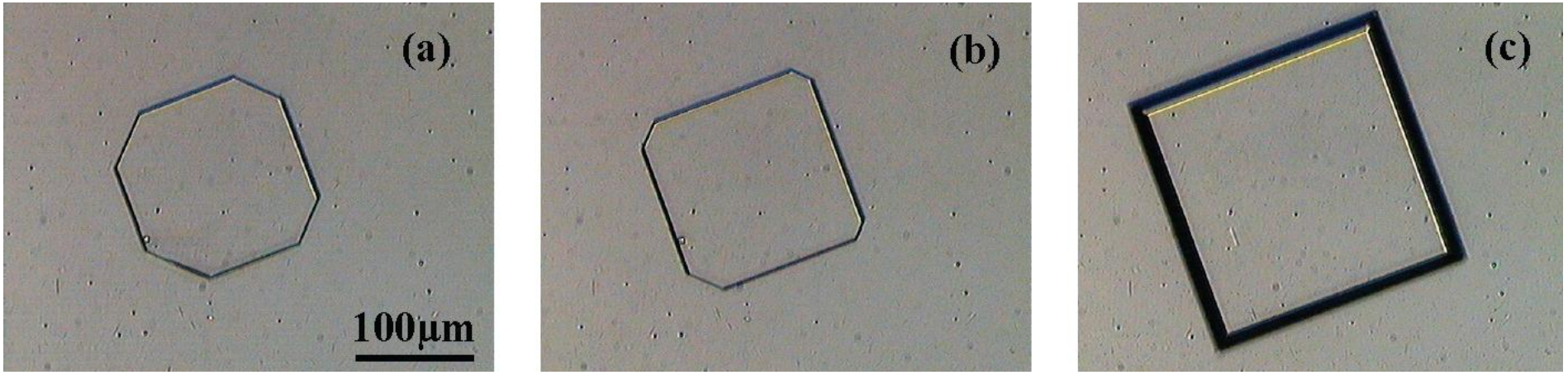

Figure 4 : Growth of a BPTI crystal in 350mM KSCN at pH=4.9 (a) to (c) are frames of a time sequence showing the evolution of the growth form. Reprinted with permission from Astier and Veesler[10]. Copyright 2008 American Chemical Society.

GROWTH MECHANISMS

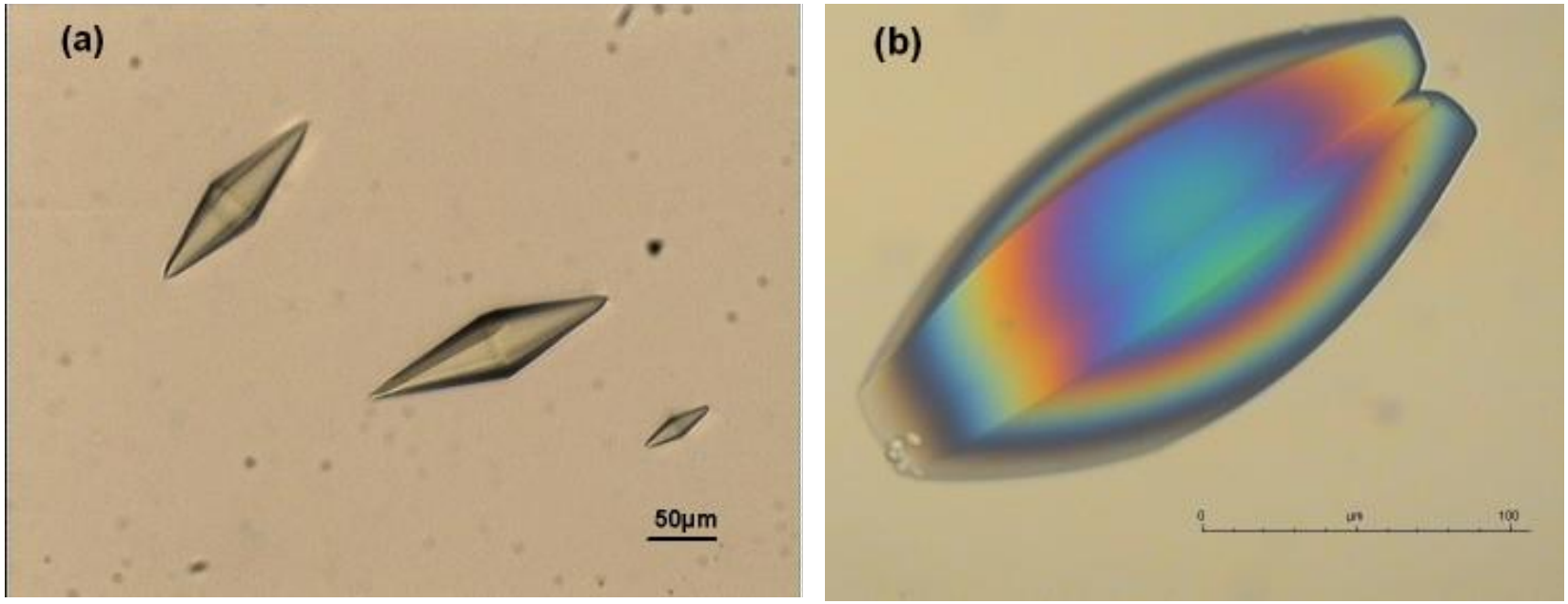

Figure 5: Crystals of BPTI at pH=4.5 in 350mM KSCN grown, (a) at low supersaturation and (b) at higher supersaturation.

2D AND SPIRAL GROWTH

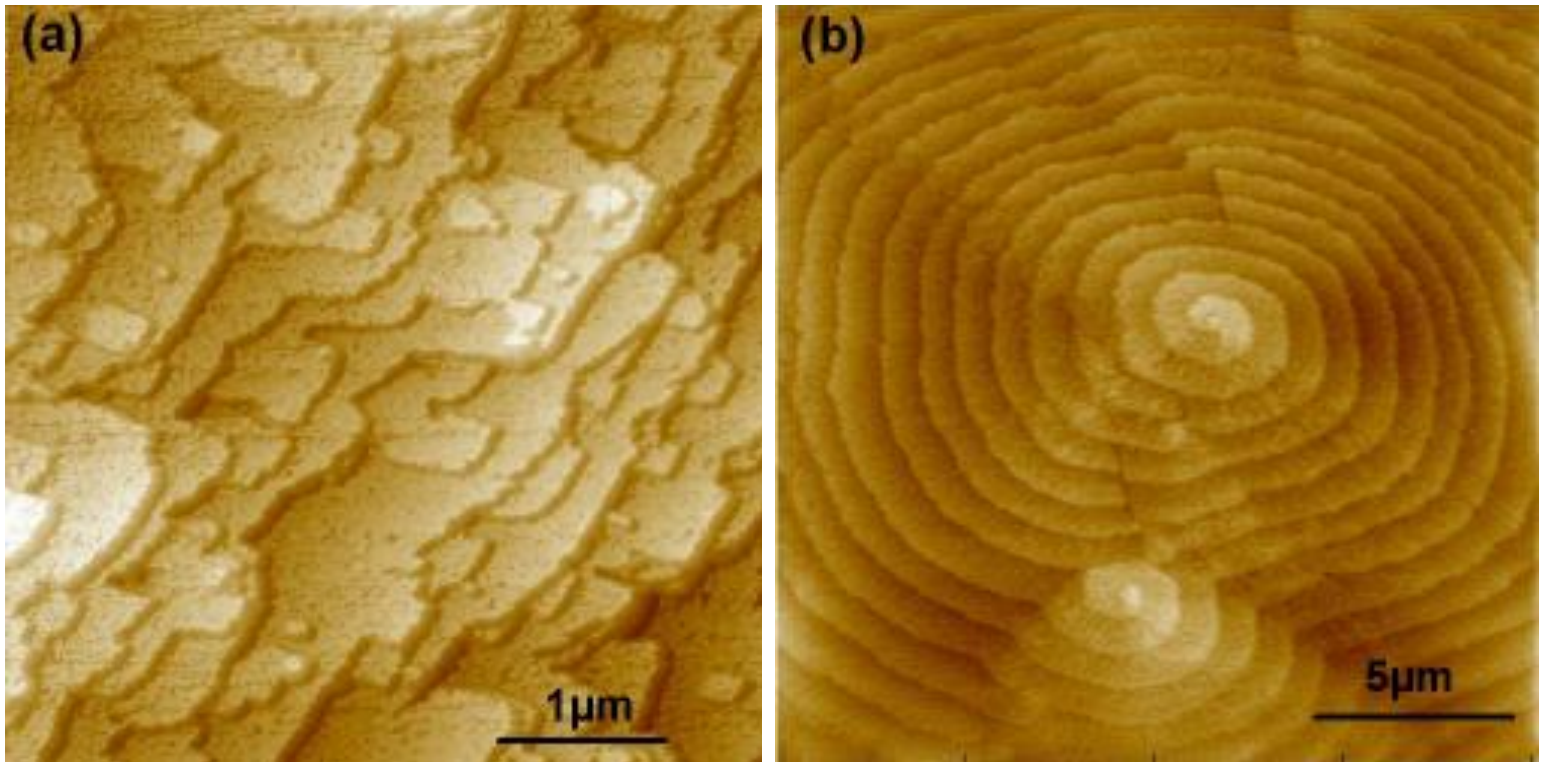

Figure 6 : AFM images showing surfaces of α-amylase, (a) 2D islands and (b) spirals after Astier et al.[61].

PHASES AND POLYMORPHISM, THE CRYSTAL FAMILY

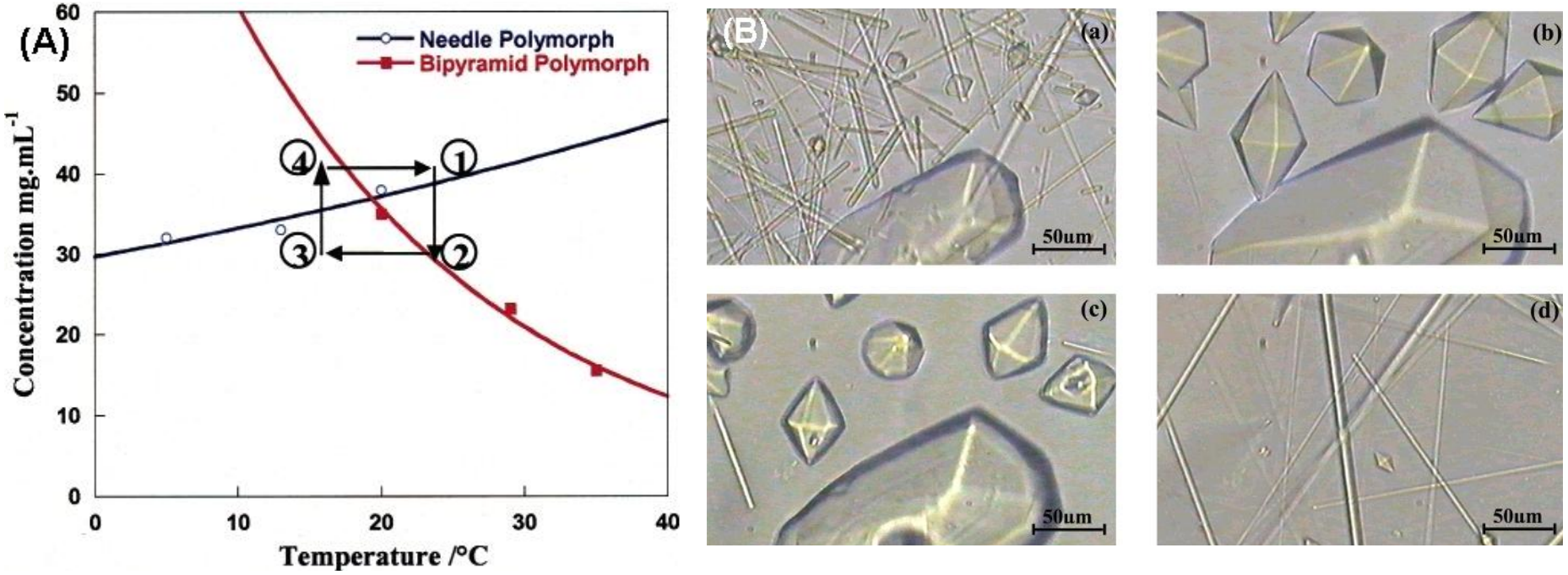

Figure 7: (A) Solubility curves of the two BPTI polymorphs in 2M NaBr versus temperature at pH 4.75. Solid lines are exponential extrapolations and are guidelines. (B) In situ observation under optical microscopy of the different stage of the BPTI phase transition; (a) mixture of BP and NP crystals in suspension (point 1 in fig.7A), (b) BP in suspension (point 2 in fig.7A), (c) dissolution of BP and nucleation and growth of NP (between point 3 and 4 in fig.7A) and (d) growth of NP and nucleation and growth of BP (between point 4 and 1 in fig.7A). Reprinted with permission from Veesler et al.[66]. Copyright 2004 American Chemical Society.

LIQUID-LIQUID PHASE SEPARATION

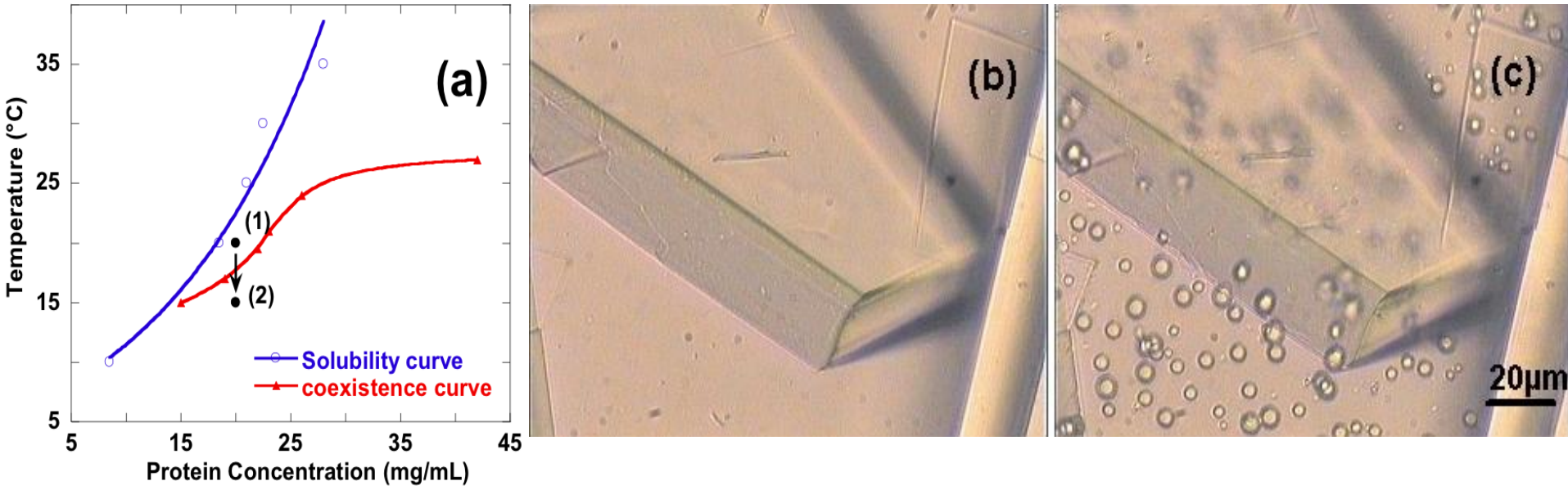

Figure 8: (a) Phase diagram for BPTI (350 mM KSCN at pH=4.9). Open circles: solubility of monoclinic BPTI from Lafont et al.[80]. Triangles: cloud point data from Grouazel et al.[75] Observation by optical microscopy of droplets of the protein rich phase in a supersaturated solution of BPTI (20 $mg.ml^{-1}$, 350 mM KSCN, pH = 4.9) when decreasing the temperature: (b) T = 20°C and (c) T = 15°C, after Grouazel et al.[75]. Reproduced with permission of the International Union of Crystallography.

OSWALD RIPENING AND KINETIC RIPENING

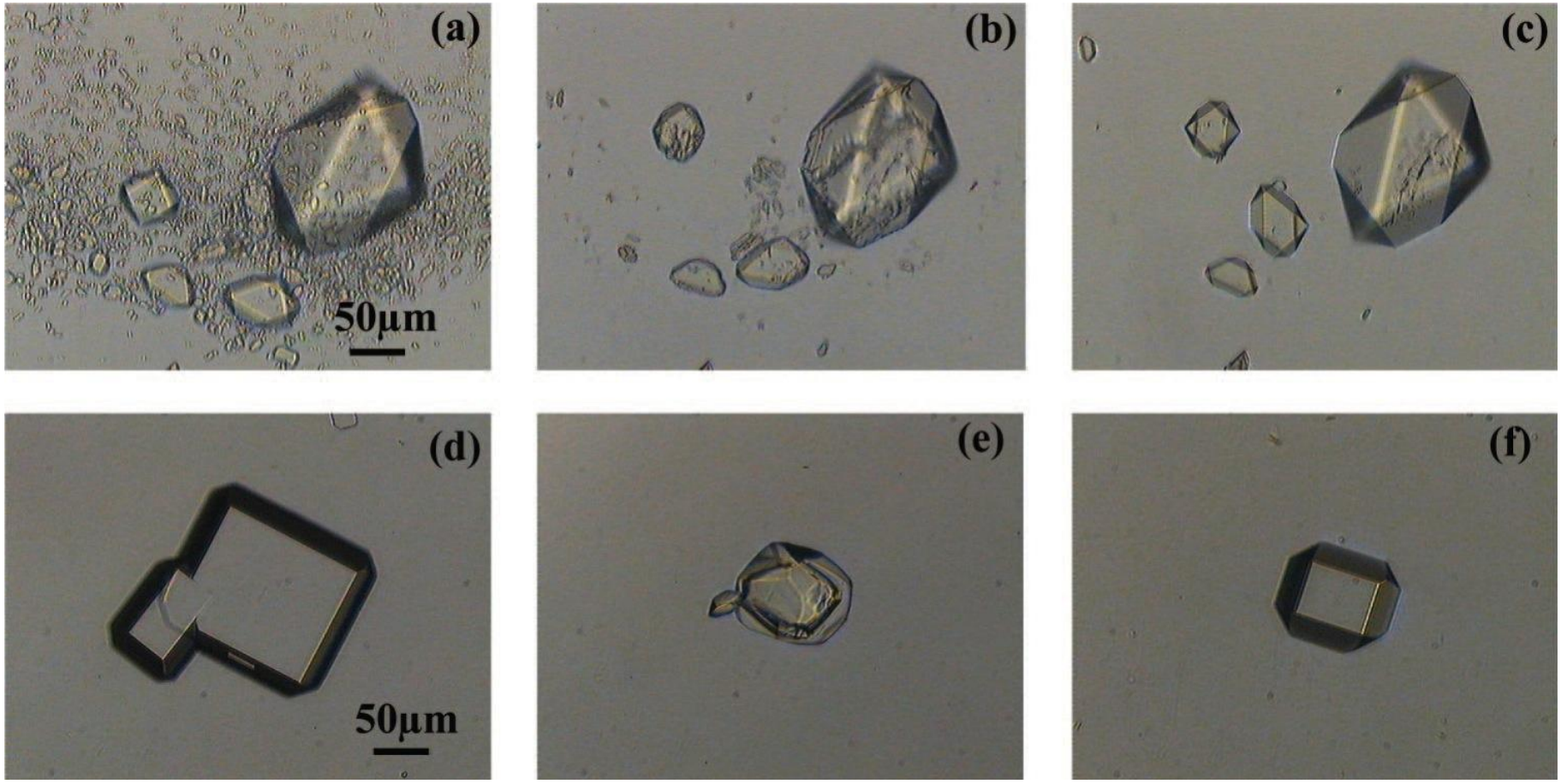

Figure 9: Kinetic ripening of B polymorph of α-amylase crystals shown in (a), by (b) partial dissolution and (c) regrowth. Elimination of a macrodefect observed in (d) by (e) dissolution and (f) growth. Reprinted with permission from Astier and Veesler[10]. Copyright 2008 American Chemical Society.

POLYMORPHISMS: A PERSPECTIVE

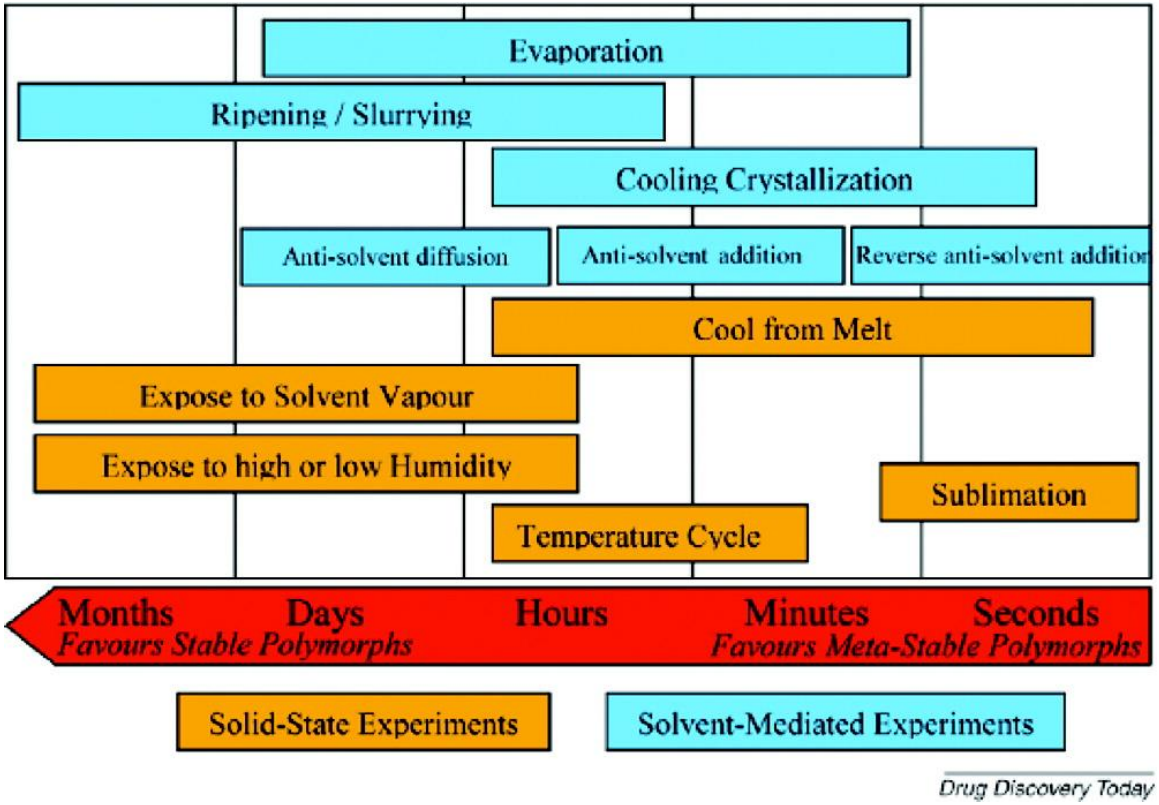

Time frames for various crystallization techniques (from ref 36, with permission. Copyright 2008 Elsevier).

Published in: Joel Bernstein; *Crystal Growth & Design* **2011,** 11, 632-650.
DOI: 10.1021/cg1013335

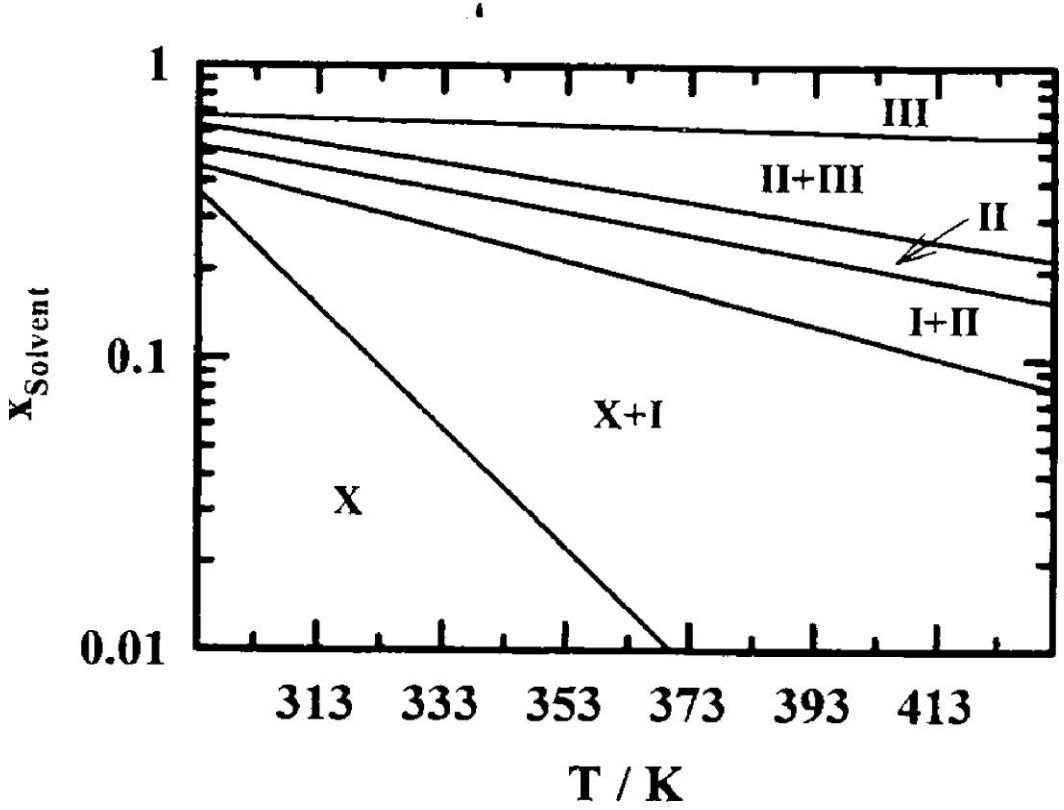

Demonstration of control over polymorphic form obtained through crystallization via supercritical CO2 an anticancer quinazoline derivative. Forms I−III were known prior to the experiment. Form X was discovered in the course of the experiment (from ref 42). Form II was most prized.

Published in: Joel Bernstein; *Crystal Growth & Design* **2011,** 11, 632-650.
DOI: 10.1021/cg1013335

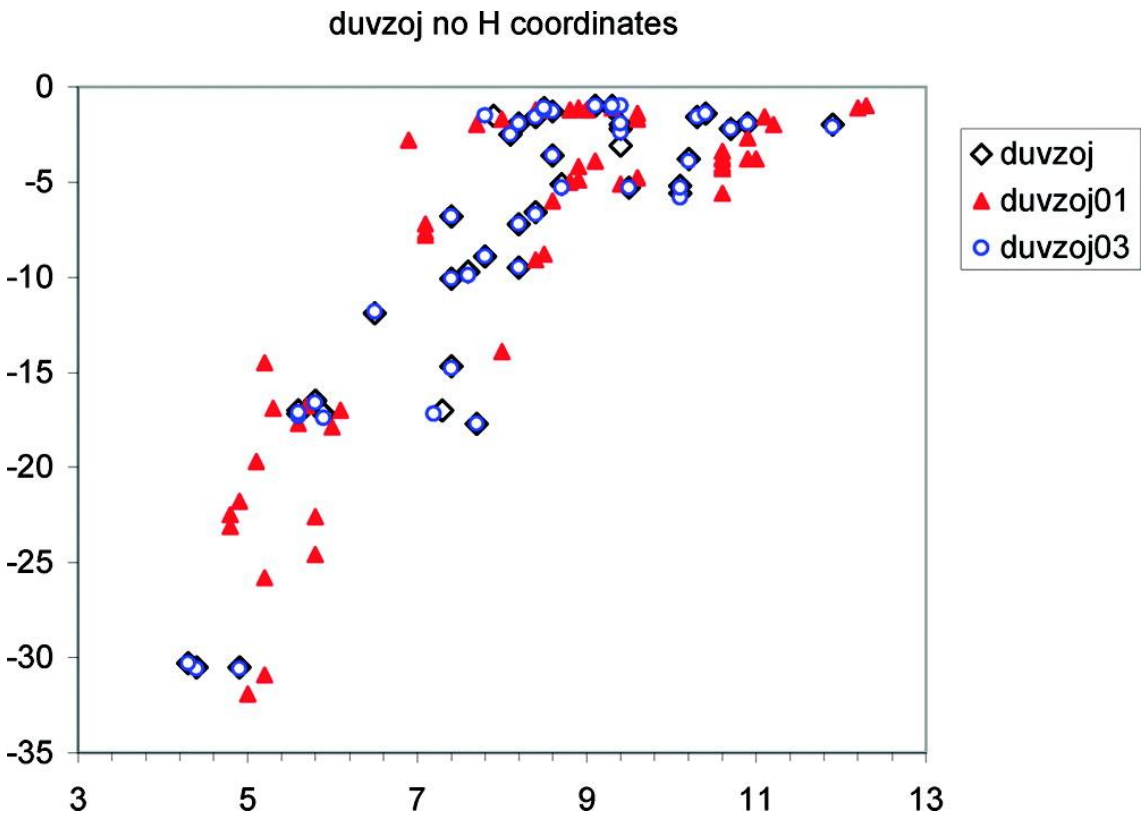

A typical example of a distance/energy plot. The horizontal axis is the distance between molecular centers of mass (Å); the vertical axis is molecule−molecule interaction energy calculated by the 6-exp UNI atom−atom potential function.(136, 137) The intermolecular energies for the structures with refcodes DUVZOJ and DUVZOJ03 are clustered, indicating that they are the same form, while those for DUVZOJ01 exhibit a different distribution, indicating a different polymorphic structure (from ref 135, with permission).

Published in: Joel Bernstein; *Crystal Growth & Design* **2011,** 11, 632-650.
DOI: 10.1021/cg1013335

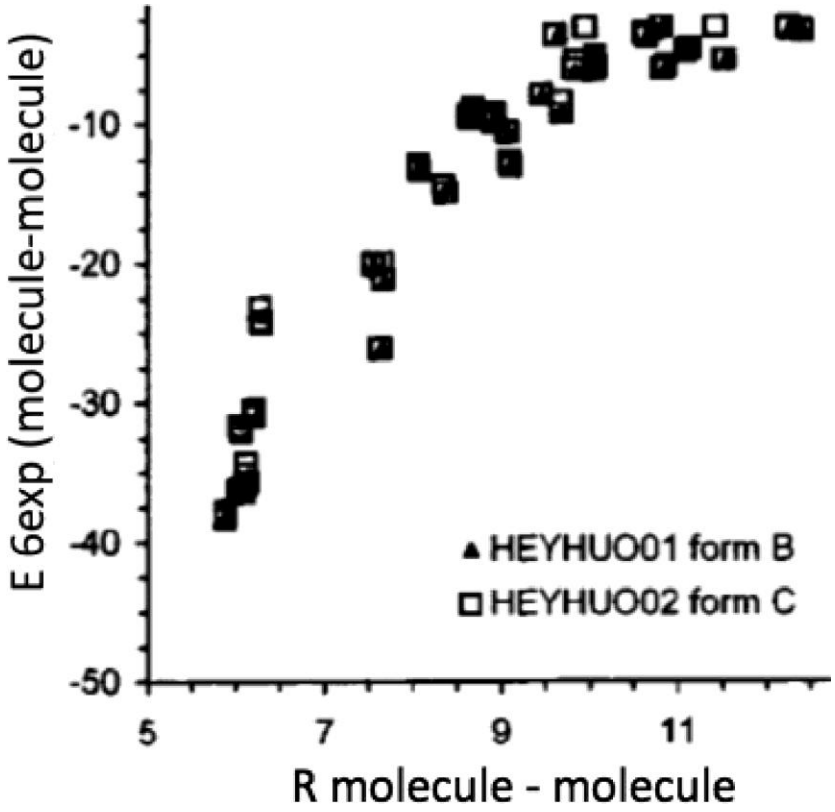

R/*E* (distance−energy) plots for Form B of HEYHUO01 (Z' = 4) and Form C HEYHUO02 (Z' = 12) (from ref 135, with permission).

Published in: Joel Bernstein; *Crystal Growth & Design* **2011,** 11, 632-650.
DOI: 10.1021/cg1013335

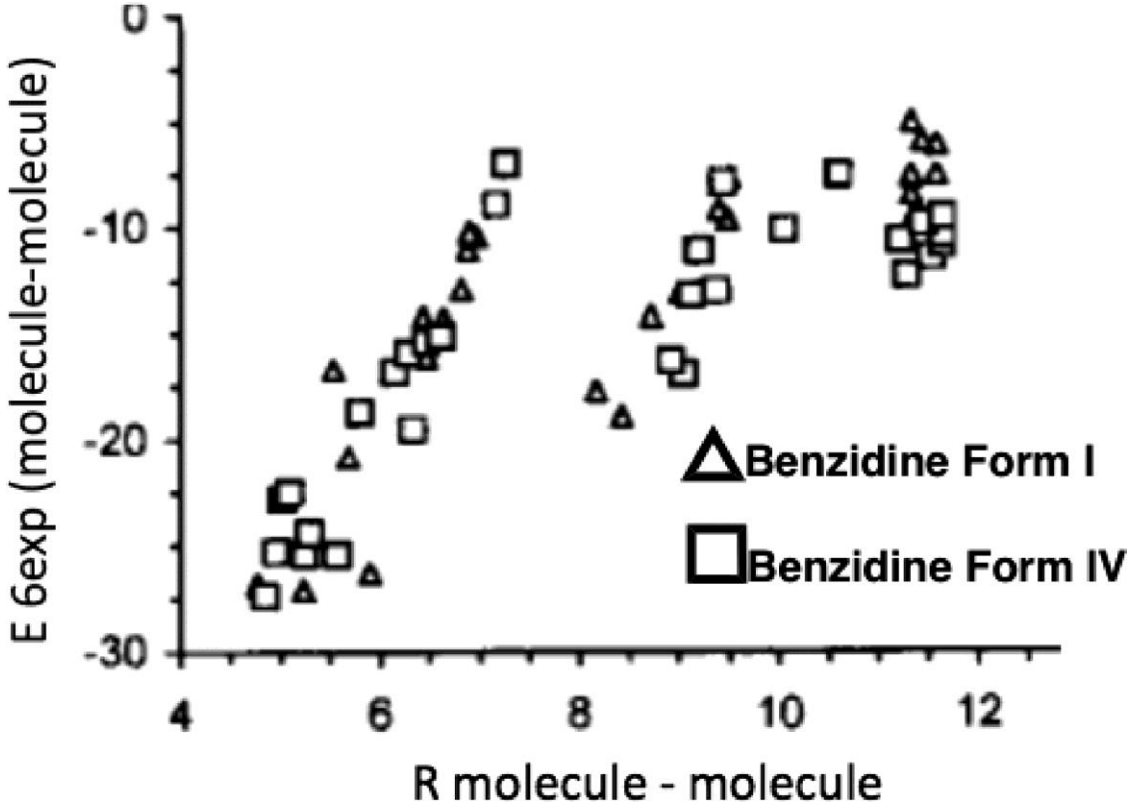

R/E (distance−energy) plots for the two polymorphs of benzidine with $Z' = 4.5$ (from ref 135, with permission).

Published in: Joel Bernstein; *Crystal Growth & Design* **2011,** 11, 632-650.
DOI: 10.1021/cg1013335

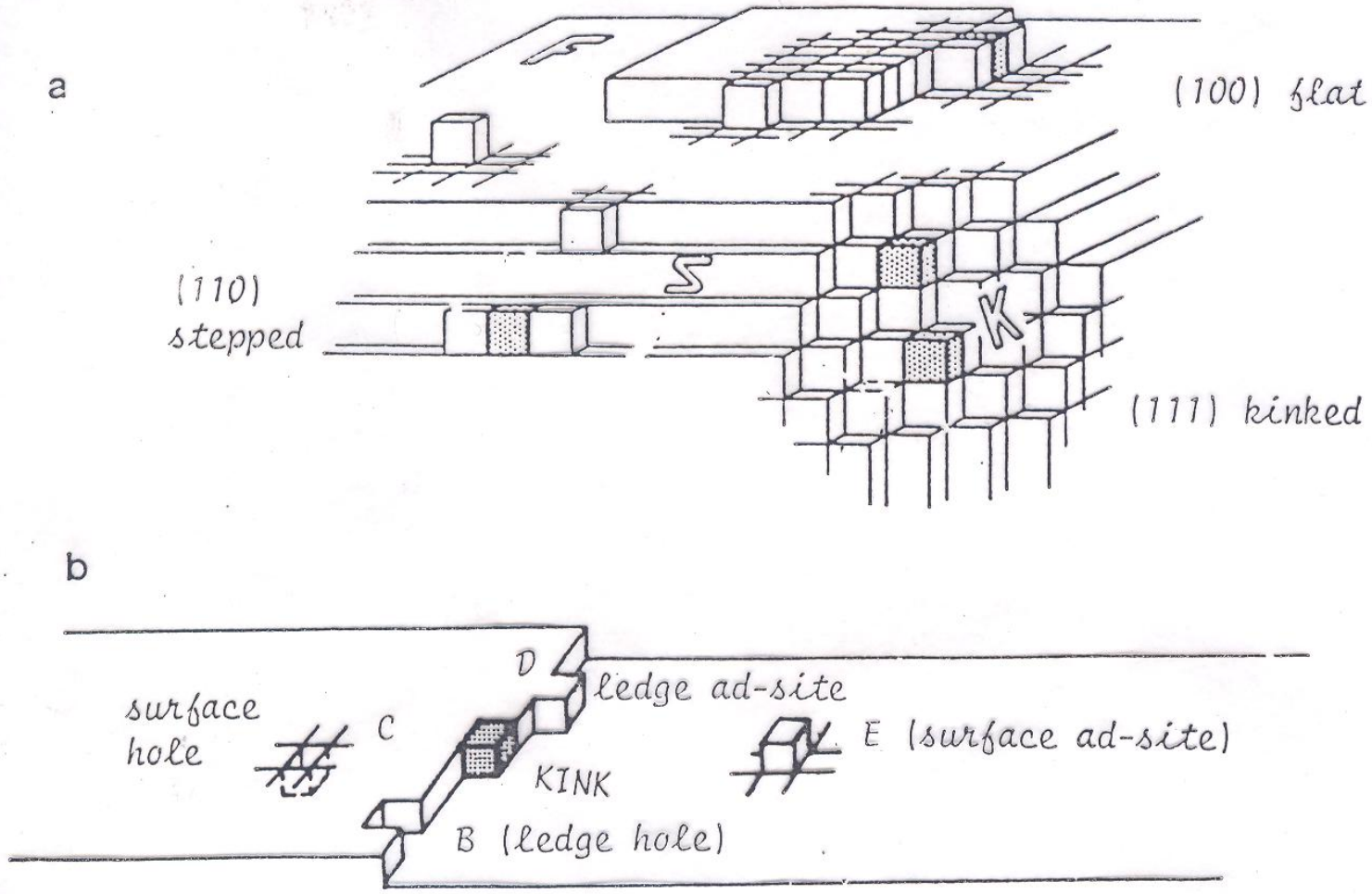
a
F
(100) flat
S
(110)
stepped
K
(111) kinked
b
D
ledge ad-site
surface
hole
C
E (surface ad-site)
KINK
B (ledge hole)

Figure 2

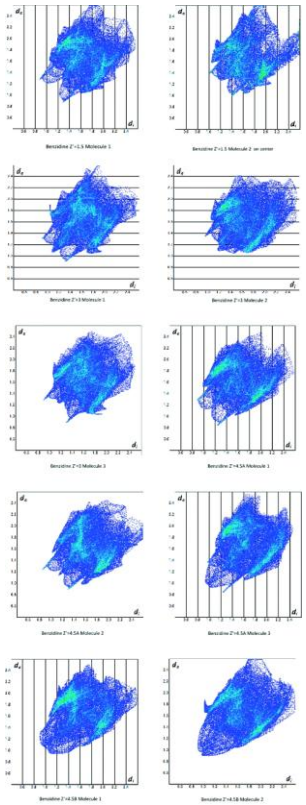

Hirshfeld fingerprint plots for the 15 different molecules in the four polymorphs of benzidine. The molecular numbering is the same as that given in the original publication.(46)

Published in: Joel Bernstein; *Crystal Growth & Design* **2011,** 11, 632-650.
DOI: 10.1021/cg1013335

Solubility curves of lysozyme crystals

Interferometry can be a strong tool to determine solubility curves of protein crystals.

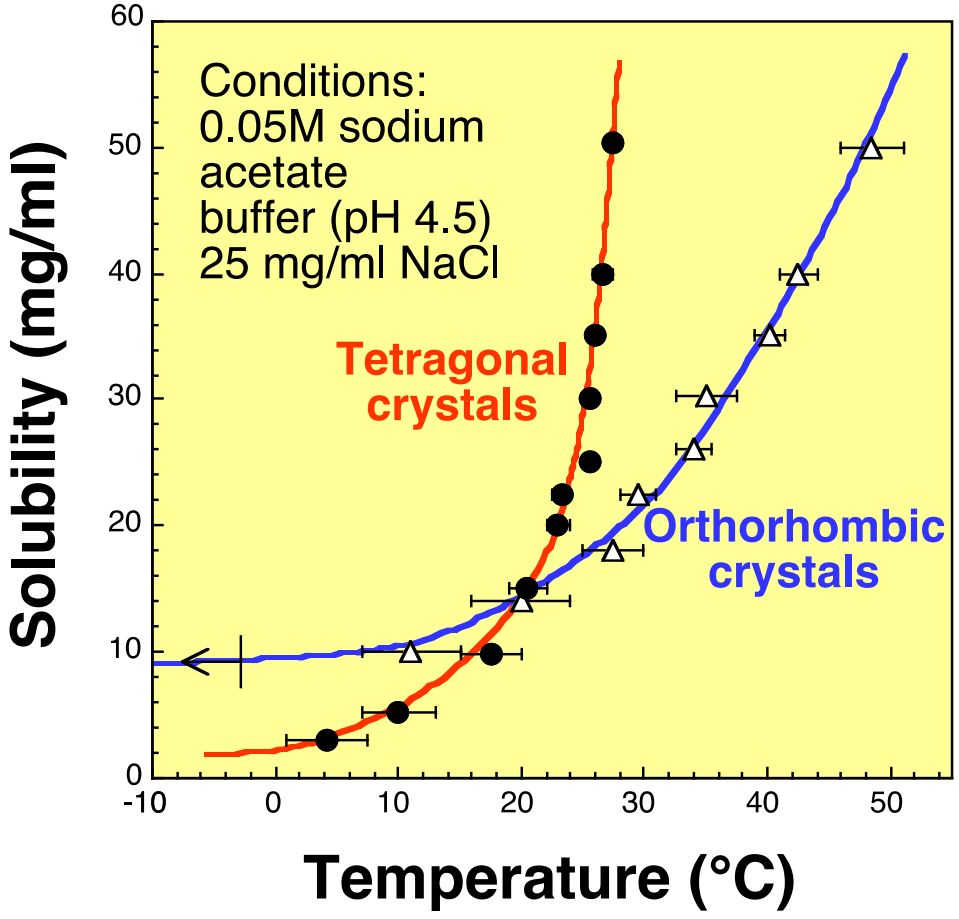

Advantages

1) **Quick** (60-100 min): 5-10 times faster than other methods.

2) **Small sample volume** (min. 10μl)

3) Applicable for a **mestable phase**

4) Including both **growth & Dissolution** processes

5) **Small impurity effect:** including dissolution process

6) **In-situ observation**

Disadvantages

Following items are necessary:

1) Temperature dependency of the solubility

2) Size of crystals (> 100 μm) (cluster of small crystals: OK)

3) Transparent solution

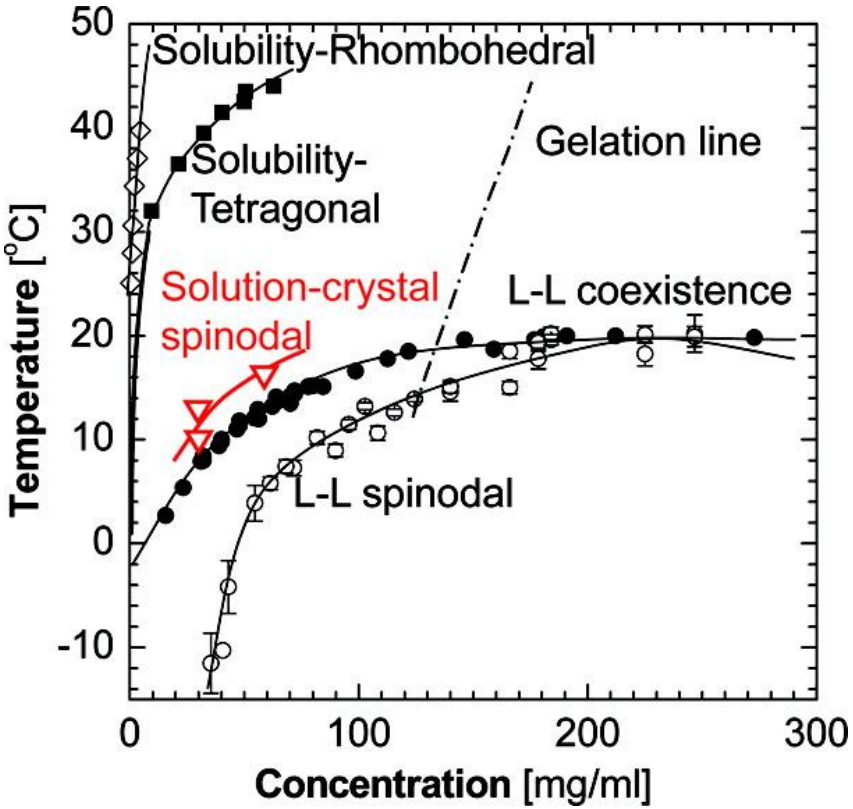

The phase diagram of a lysozyme solution determined experimentally in 0.05 M Na acetate buffer at pH = 4.5 and 4.0% NaCl. Liquidus, or solubility lines—from refs 108 and 109 liquid−liquid (L−L) coexistence and respective spinodal—from ref 25, gelation line—from refs 24 and 25. Solution−crystal spinodal is highlighted in red and is from ref 81.

Published in: Peter G. Vekilov; *Crystal Growth & Design* **2010,** 10, 5007-5019.
DOI: 10.1021/cg1011633

Estudios de nucleación y crecimiento cristalino de proteínas: cristalización de ferritina bajo la influencia de un campo eléctrico interno

Andrea Elizabeth Gutiérrez Quezada
Asesor: Dr. Abel Moreno Cárcamo
Laboratorio Bioquímica 3

Ferritina

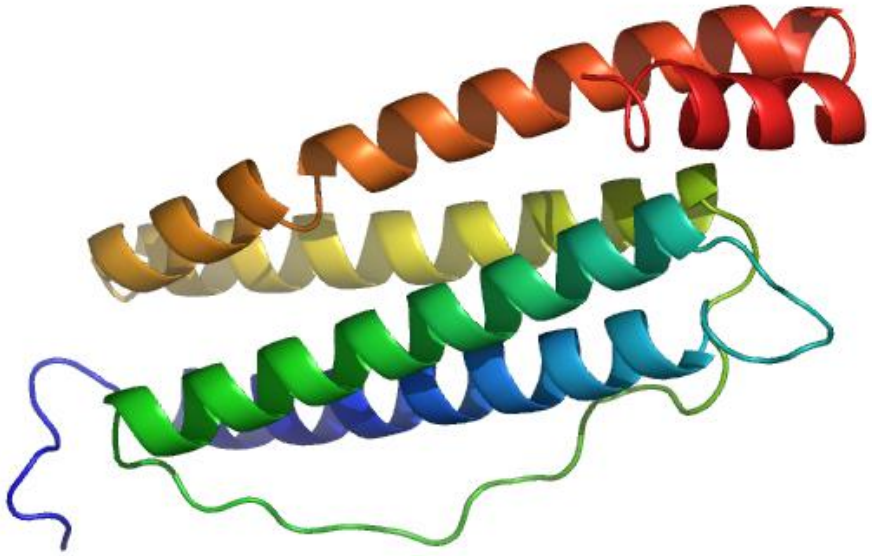

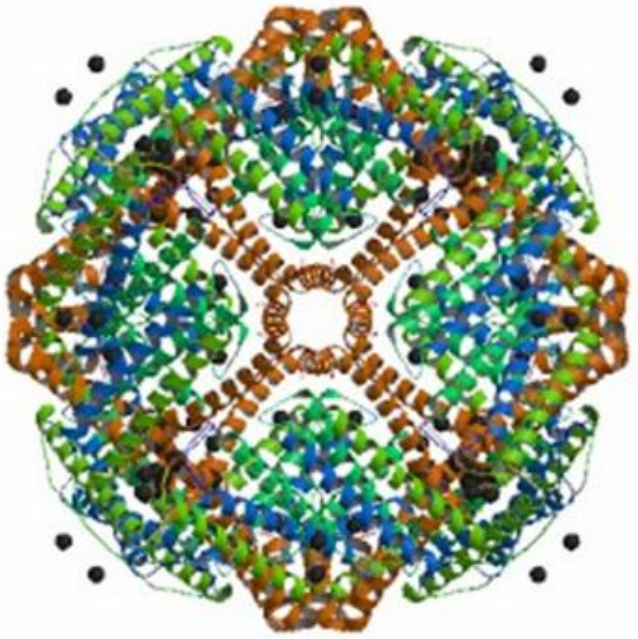

Andrea E. Gutiérrez Quezada

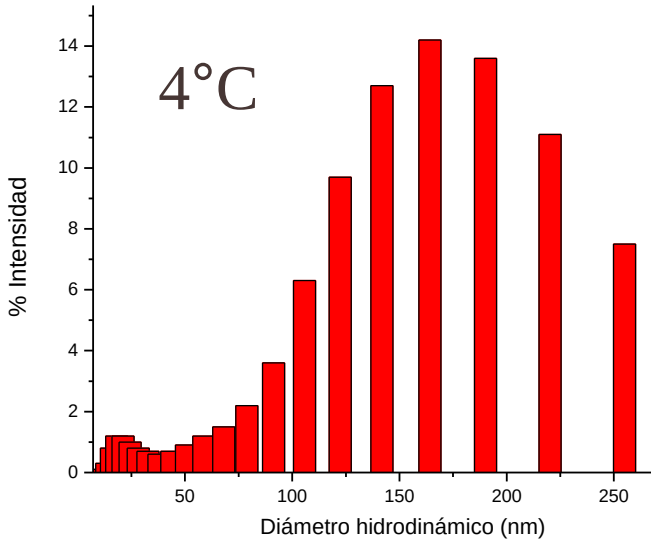

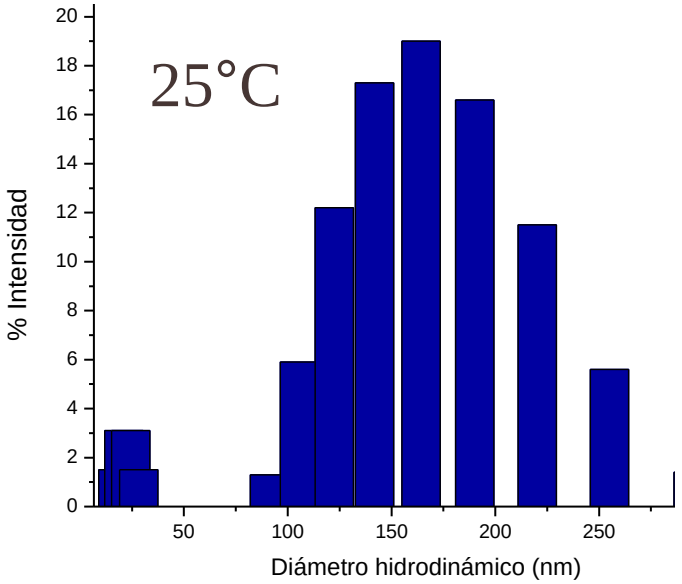

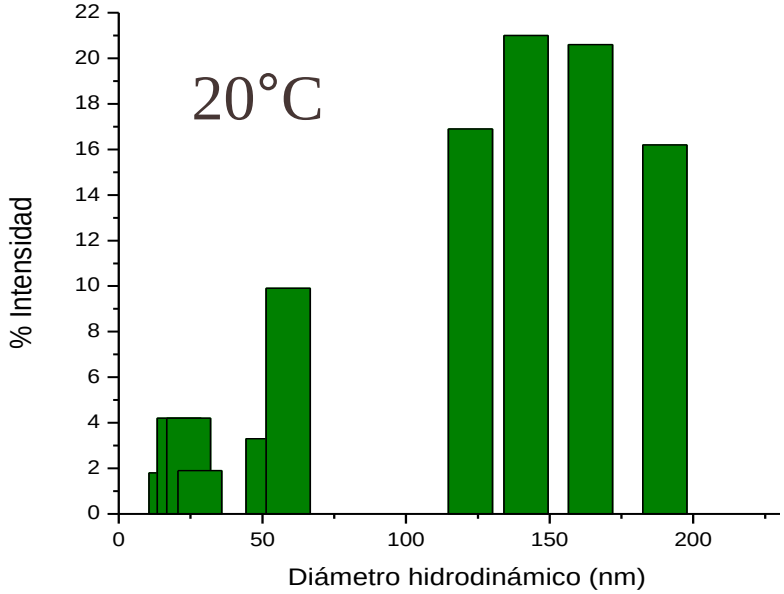

Andrea E. Gutiérrez Quezada

- **Resultados**
- Análisis
- Conclusiones

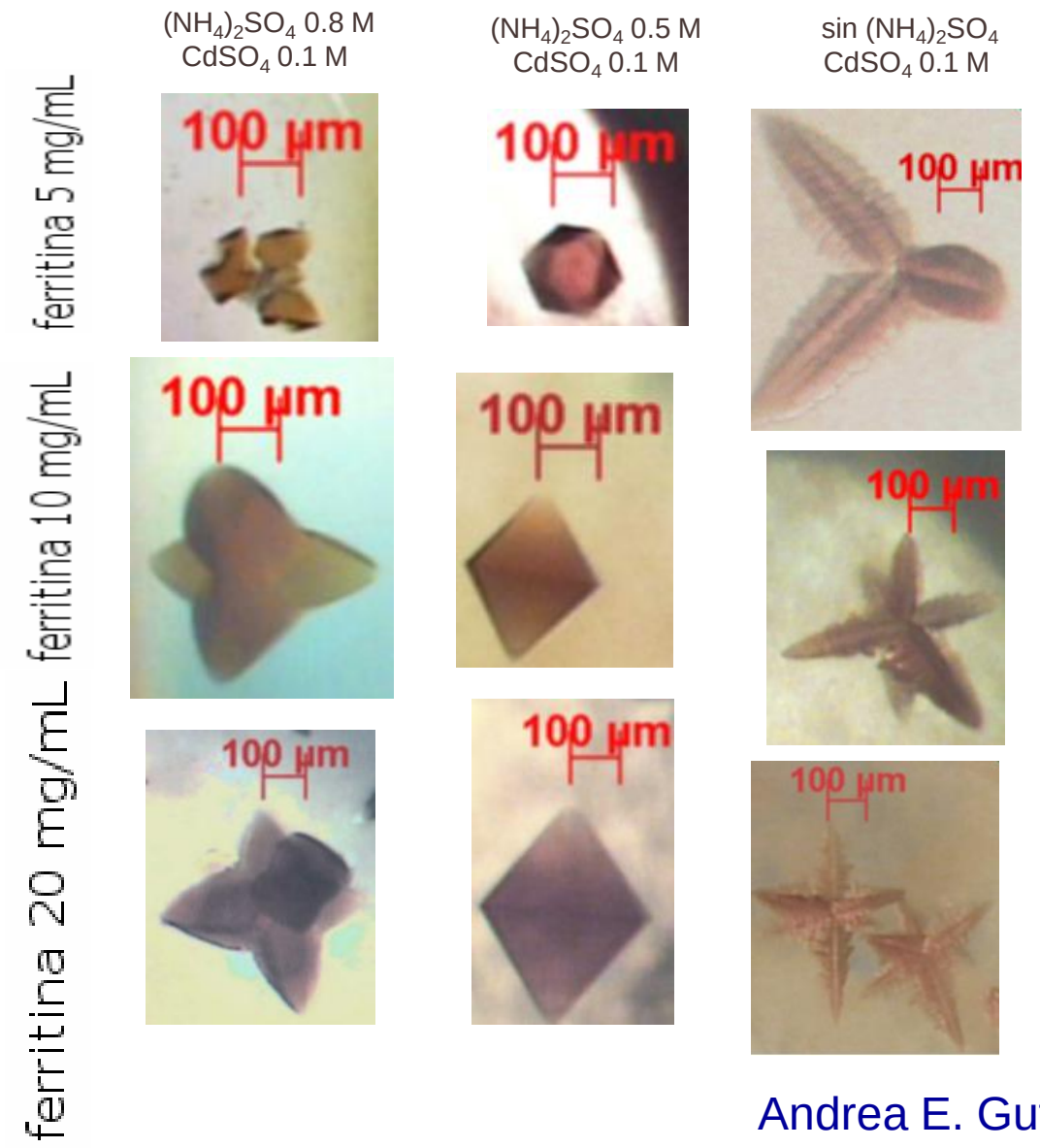

POLYMORPHISM IN A TOLL PROTEIN

As a ***Brevia*** in **Science (Submitted April 2012)**

Liesegang patterns of Toll receptor crystals grown in gel

By Monique Gangloff [1], Abel Moreno [2], Nick J. Gay

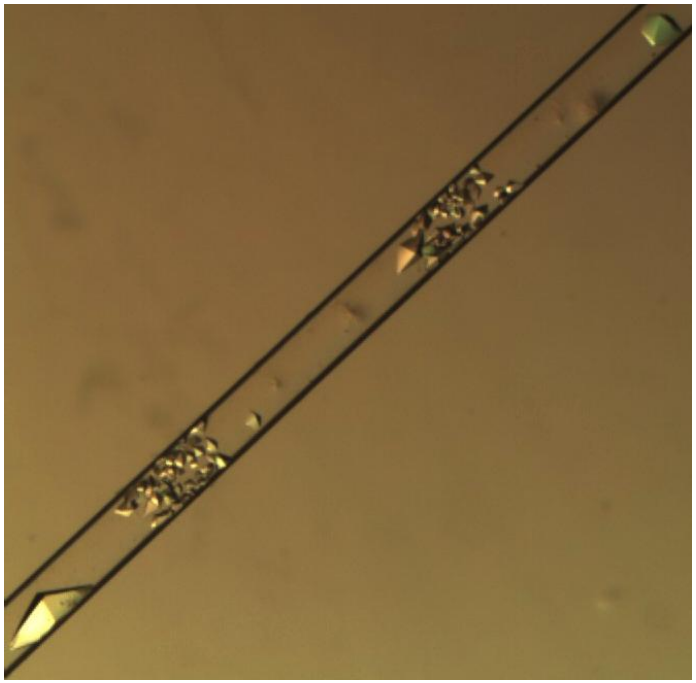

Figure 1. Liesegang rings obtained with the counter-diffusion method in a capillary tube using agarose gel in which Toll periodically crystallized.

Table S1. Data collection and refinement statistics

	Native	Derivative
Data collection		
Wavelength	29.95-2.41	47.00-3.00
Space group	$P2_12_12_1$	$P4_32_12$
Cell parameters		
a, b, c (Å)	88.79 93.28 225.34	87.64 87.64 220.74
α, β, γ (°)	90.0 90.0 90.0	90.0 90.0 90.0
Molecules per A.U.	4	2
Matthews coefficient	3.29	2.99
Solvent content (%)	62.59	58.82
Resolution (Å)	29.9-2.41 (2.54-2.41) [a]	47.40-3.00 (3.16-3.00) [a]
No. observations	481766	234278
No. unique reflections	72966	18063
R_{merge} (%) [b]	0.056 (0.542) [a]	0.138 (0.653) [a]
I/σ(I)	20.6 (3.0) [a]	14.1 (3.4) [a]
Completeness (%)	99.3 (97.1) [a]	99.9 (100.0) [a]
Mean multiplicity	6.6 (6.0) [a]	13.0 (12.0) [a]
Refinement		
Resolution (Å)	29.9-2.41	47.4-3.0
No. reflections (total)	72763	17997
No. reflections (test)	3668	918
R_{work} (%) [c]	20.16	25.40
R_{free} (%) [d]	21.69	28.02
No atoms	9299	4414
Protein	8716	4340
Heterogen atoms	579	74
Waters	333	0
Mean B ($Å^2$)	66.50	64.40
R.m.s. deviations		
Bond lengths (Å)	0.008	0.007
Bond angles (°)	0.97	0.93
Molprobity [e]		
Clashscore, all atoms	6.02 (99^{th} percentile)	12.38 (97^{th} percentile)
Molprobity score	1.72 (98^{th} percentile)	2.48 (95^{th} percentile)
Ramachandran statistics		
Favoured	94.2	93.7
Outliers	0.0	0.0